Mechanisms and plasticity of chemogenically induced interneuronal suppression of principal cells

Stephanie Rogers[a,1], Peter A. Rozman[a,b,1], Manuel Valero[a], Werner K. Doyle[b], and György Buzsáki[a,c,d,2]

[a]Neuroscience Institute, Langone Medical Center, New York University, New York, NY 10016; [b]Department of Neurosurgery, Langone Medical Center, New York University, New York, NY 10016; [c]Department of Neurology, Langone Medical Center, New York University, New York, NY 10016; and [d]Center for Neural Science, New York University, New York, NY 10003

Edited by Marcus E. Raichle, Washington University in St. Louis, St. Louis, MO, and approved November 19, 2020 (received for review July 13, 2020)

How do firing patterns in a cortical circuit change when inhibitory neurons are excited? We virally expressed an excitatory designer receptor exclusively activated by a designer drug (Gq-DREADD) in all inhibitory interneuron types of the CA1 region of the hippocampus in the rat. While clozapine N-oxide (CNO) activation of interneurons suppressed firing of pyramidal cells, unexpectedly the majority of interneurons also decreased their activity. CNO-induced inhibition decreased over repeated sessions, which we attribute to long-term synaptic plasticity between interneurons and pyramidal cells. Individual interneurons did not display sustained firing but instead transiently enhanced their activity, interleaved with suppression of others. The power of the local fields in the theta band was unaffected, while power at higher frequencies was attenuated, likely reflecting reduced pyramidal neuron spiking. The incidence of sharp wave ripples decreased but the surviving ripples were associated with stronger population firing compared with the control condition. These findings demonstrate that DREADD activation of interneurons brings about both short-term and long-term circuit reorganization, which should be taken into account in the interpretation of chemogenic effects on behavior.

DREADDs | interneurons | perturbation | hippocampus | sharp wave ripples

The chemogenetic technology DREADD (designer receptors exclusively activated by designer drugs) is a widely used experimental method to control neuronal activity with an exogenous receptor that is engineered to respond selectively to an injectable agonist (1–4). In contrast to traditional pharmacology, chemogenetic techniques are both generalizable and specific because a receptor–agonist combination can be used for cell type-specific activation or inhibition of different neural populations in any brain region (4). The most prevalent DREADD platform exploits the human muscarinic receptors hM3Dq and hM4Di that are not activated by endogenous neurotransmitters but via the "designer drug" clozapine N-oxide (CNO). Subsequent experiments identified that the pharmacological actuator of CNO in the brain is the metabolically derived clozapine, arising from systemic CNO administration (4, 5). A recent improvement of the method introduced an ion channel-based platform for more potent neuronal activation and silencing that is controlled by pharmacologically selective actuator modules (6). Because of their easy use and assumed selective action, chemogenetic tools have become popular in animal research, and there is growing interest in developing chemogenetic techniques for clinical therapeutics (3).

DREADD techniques have the advantage of activating or suppressing neurons over longer time periods, allowing for testing the contribution of specific neuron classes to behavior. However, it is unlikely that CNO brings about sustained activation or suppression in all target neurons uniformly and continuously because activation of interconnected inhibitory neuron populations often brings about unpredictable effects (7–11). Long-lasting excitation or inhibition of neurons typically induces synaptic plasticity and homeostatic regulations (10–13) but such potential circuit modifications have not yet been examined in connection with DREADD.

The distal-less homeobox 5 and 6 (Dlx5/6) genes are specifically and transiently expressed by all forebrain GABAergic interneurons during embryonic development (14) and the recombinant adeno-associated virus (rAAV-hDLX) restricts gene expression to GABAergic interneurons in several species tested (15). Using rAAV-hDLX-Gq-DREADD in the hippocampus allowed us to investigate the mechanisms of chemogenetic modulation of interneuronal activity in behaving rats. CNO activation of all types of interneurons in the CA1 hippocampal region leads to a paradoxical decrease of the overall firing of many interneurons, coupled with a several-fold decrease of pyramidal cell firing. Interneurons did not display uniform sustained firing but, instead, enhanced activity of subgroups was interleaved with suppression of others. The sustained suppression of pyramidal cell activity was often interrupted by population bursts underlying sharp wave ripples. During such events, spiking of pyramidal cells was enhanced compared with control conditions. These findings demonstrate that DREADD activation of interneurons leads to dynamic circuit reorganization, which should be considered in the interpretation of chemogenic mechanisms in behavior (5, 16–21).

Results

Two weeks prior to implantation of recording silicon probes in the hippocampal region, 1,200 nL dlx5/6-Gq-DREADD AAV was infused into the CA1 pyramidal layer in adult male rats to express excitatory DREADD (hM3Dq) in all interneurons (Fig. 1*A*

Significance

Chemogenic activation of interneurons can bring about unexpected short-term and long-term changes in circuit dynamics. DREADD activation of all interneuron types suppressed firing of pyramidal cells but, unexpectedly, individual interneurons did not display sustained firing but instead undulated firing rates, interleaved with other interneurons. Despite the tonic suppression of spikes of individual pyramidal neurons, population bursts underlying sharp wave ripples persisted, often with stronger synchrony. Repeated drug application induced progressively weaker changes over days. Such plastic effects of DREADD activation should be taken into account in the interpretation of behavioral consequences.

Author contributions: G.B. designed research; S.R. performed research; S.R., P.A.R., and M.V. analyzed data; and S.R., P.A.R., W.K.D., and G.B. wrote the paper.

The authors declare no competing interest.

This article is a PNAS Direct Submission.

[1]S.R. and P.A.R. contributed equally to this work.

[2]To whom correspondence may be addressed. Email: gyorgy.buzsaki@nyulangone.org.

This article contains supporting information online at https://www.pnas.org/lookup/suppl/doi:10.1073/pnas.2014157118/-/DCSupplemental.

Published December 28, 2020.

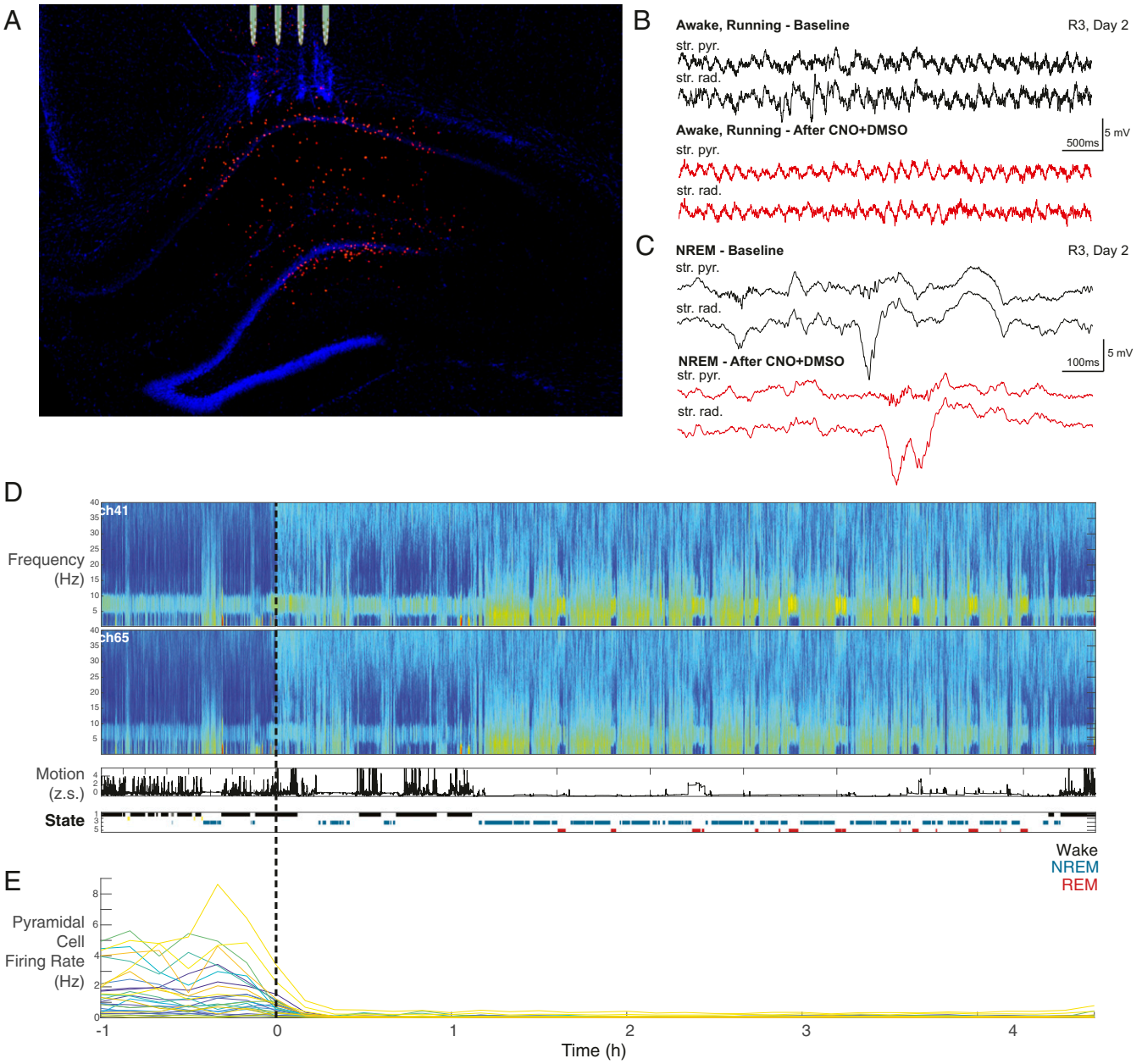

Fig. 1. Electrode implantation and data acquisition and analysis. (*A*) Histological section showing dTomato-expressing DREADD interneurons in all layers of the CA1 hippocampal region. A few interneurons in the hilus are also labeled. Tips of the silicon probe shanks are aligned with penetration tracks. (*B*) Representative LFP recording from two separate channels in the str. pyramidale and str. radiatum while running before (black) and 1 h after (red) CNO injection. (*C*) Representative LFP recording from the same two channels during non-REM (NREM) sleep with representative sharp wave ripple complexes shown. (*D*, *Top*) Multitaper spectrogram from 0 to 40 Hz of one entire session in two separate channels utilized for state scoring. Time $t = 0$ represents the time of CNO + DMSO injection. (*D*, *Middle*) Accelerometer tracing (as a *Z* score; z.s.) over the same session. (*D*, *Bottom*) Automatic state scoring of the same session. States are coded as listed (*Right*). (*E*) Pyramidal cell firing rates over the same session. Each cell is represented by a different-colored trace. Note the uniform decrease in firing rate shortly after injection.

and *SI Appendix*). Previous histological evaluation has shown that virus infection included all interneuron types in all layers of the CA1 region spanning from the dorsal to the posterior hippocampal segment (Fig. 1*A*) (15). Interneurons in minor parts of the dorsal blade of the dentate/hilus region were also labeled in some animals (Fig. 1*A*).

Daily neurophysiological recordings started at a fixed time each morning while the animal was freely behaving or sleeping in its home cage (Fig. 1 *B* and *C*). During the first hour, baseline recordings were obtained (baseline control), after which the animal received an intraperitoneal injection of either 5 mg/kg CNO in 1% dimethyl sulfoxide (DMSO) or only the 1% DMSO (vehicle control) and recordings continued for 4 to 12 h. Hippocampal local field potential (LFP), movement, and electromyogram were used to classify brain states into wake (immobility and walking) and sleep (non-REM [non-rapid eye movement] and REM) epochs (Fig. 1*D*) (22). Units were isolated and classified into putative pyramidal cells ($n = 875$ in eight rats) and interneurons ($n = 90$; *SI Appendix*). The remaining unclassified neurons ($n = 31$ in CNO and 4 in DMSO sessions) were excluded

from further analysis. We have not observed obvious overt behavioral changes in any of our animals after central nervous system injection. However, we cannot exclude the possibility that engagement in hippocampus-dependent tasks may reveal deficits in specific cognitive tasks.

Firing Patterns of Pyramidal Cells and Interneurons. Administration of CNO led to a several-fold suppression of the firing of the recorded pyramidal neurons. Suppression of firing began within 5 min of the intraperitoneal injection and remained significantly below baseline activity throughout the recording session (Figs. 1*E* and 2 *A* and *B*; $P = 8.1\text{e-}70$; paired t test). Unexpectedly, the mean firing rate of the recorded putative interneuronal population also decreased after CNO (Fig. 2 *A* and *B*) and so did the total number of action potentials of all interneurons per unit time. The observed changes were not a consequence of the behavioral and/or brain state changes of the animals after CNO administration because selective comparisons of log firing rates confined to preclassified wake and REM and non-REM epochs showed similar results: significant suppression of pyramidal cells and variable overall responses of individual interneurons in all brain states (*SI Appendix*, Fig. S1). Vehicle (DMSO) injection in control sessions ($n = 14$) did not affect the overall firing rates (Fig. 2 and *SI Appendix*, Fig. S1).

In an attempt to search for sources of neuronal heterogeneity, we classified both pyramidal cells and interneurons into three groups: CNO-induced decrease, CNO-induced increase, or no firing rate change (*SI Appendix*, Fig. S2 *A* and *C*). Although the predrug firing rates of these neurons were different from each other, as expected by the long-term preservation of firing rates (23), they were indistinguishable by their spike waveform or bursting properties.

While the pyramidal cell population was uniformly suppressed, interneurons varied both in their responses and their post-CNO temporal dynamics (Fig. 3*A*). Of the 90 interneurons, 39% decreased their firing rates significantly (*Materials and Methods*) during the first hour of CNO effect, whereas only 13% showed a significant overall increase (*SI Appendix*, Fig. S2). Several interneurons were highly active for various bouts of time epochs, preceded and followed by reduced firing rates (Fig. 3*A* and *SI Appendix*, Figs. S3 and S4). Thus, suppression of the pyramidal neuronal activity was achieved not by sustained increased activity of all interneurons or a special subset but by a perpetually changing interleaved activity of interneurons. These

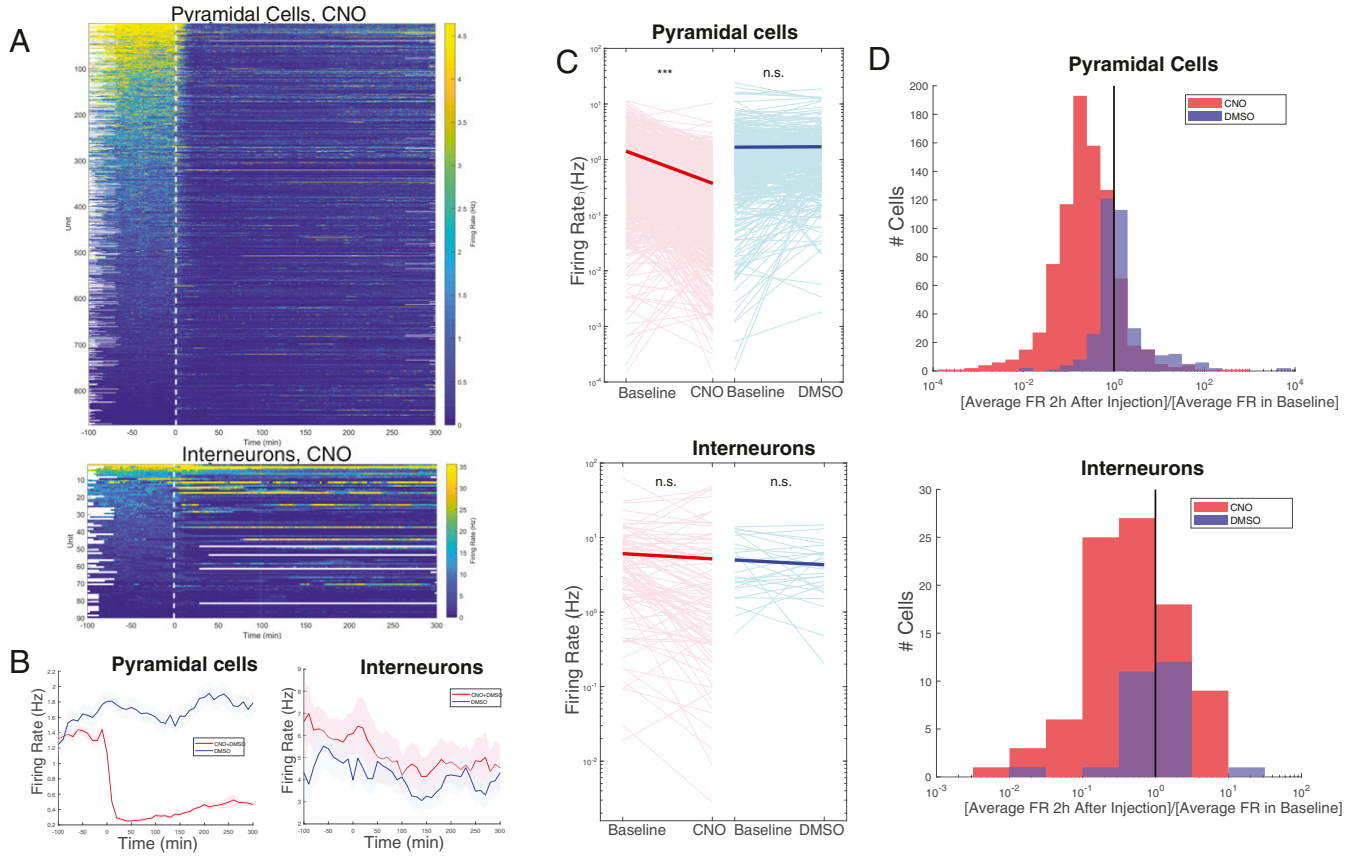

Fig. 2. Pyramidal cell firing rate reliably decreases following injection of CNO, while interneurons respond heterogeneously. (*A*) Firing rate over time for pyramidal cells (*Top*) and interneurons (*Bottom*) in CNO + DMSO sessions ($n = 36$). Injection occurs at time $t = 0$. Each line is the color-coded firing rate of a neuron, averaged over successive nonoverlapping 60-s windows. White areas indicate no recordings in those time epochs, as some sessions were longer than others. (*B*) Average firing rate over time for all pyramidal cells (*Left*) and all interneurons (*Right*) in CNO + DMSO (red) or DMSO-only (blue) sessions. Shaded areas represent SEM. Firing rates were first calculated over successive nonoverlapping 600-s windows and subsequently averaged across cells. CNO + DMSO sessions: $n = 875$ pyramidal cells and 90 interneurons. DMSO (control) sessions: 366 pyramidal cells and 29 interneurons. (*C*) Changes in firing rate from baseline to the first 2 h after injection of either CNO + DMSO (red; *Left*) or DMSO only (blue; *Right*) for individual pyramidal cells (*Top*) and interneurons (*Bottom*). Individual changes are represented by light pink and light blue lines, while averaged change is represented by the thick red or blue lines. Changes were significant only for pyramidal cells in CNO + DMSO ($P = 7.03 \times 10{-}86$). ***$P < 0.0001$; n.s., not significant. (Other P values: pyramidal cells, DMSO only, $P = 0.72$; interneurons, CNO + DMSO, $P = 0.32$; DMSO only, $P = 0.28$.) (*D*) Histogram of the ratio of the firing rates in *C*. (*D*, *Top*) Pyramidal cells. (*D*, *Bottom*) Interneurons. CNO + DMSO is indicated in red; DMSO only is indicated in blue. FR, firing rate.

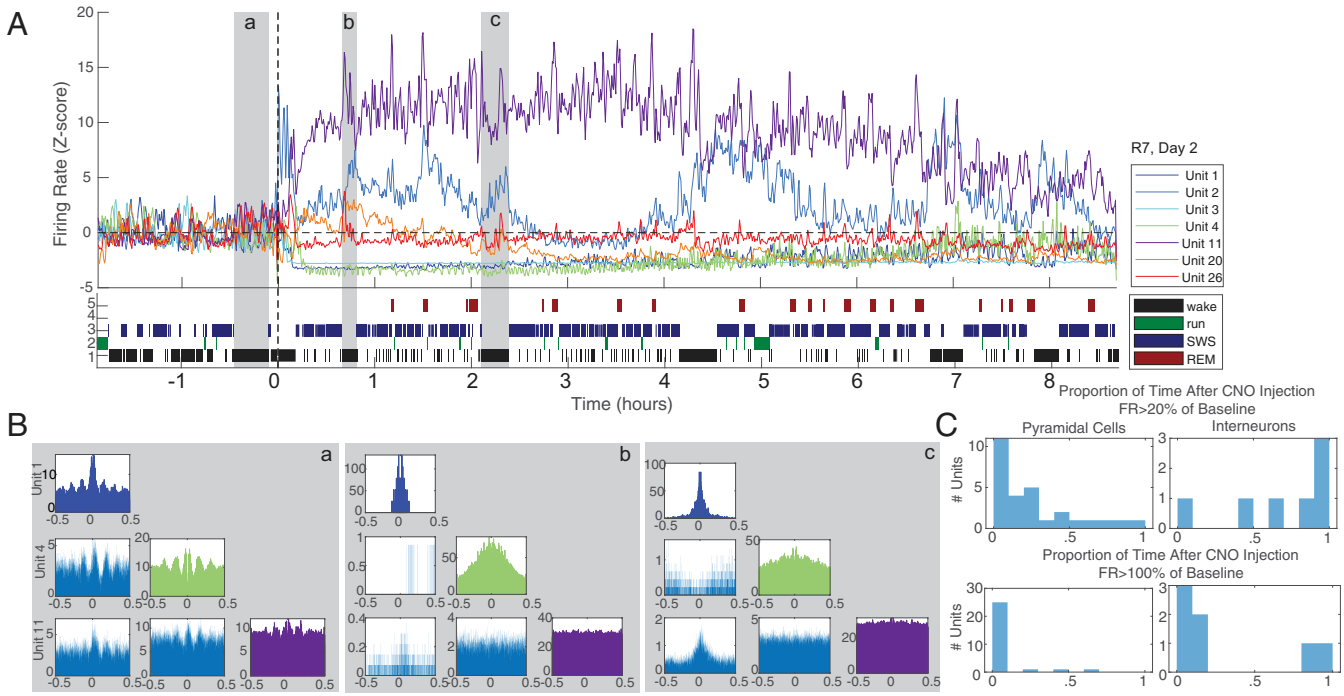

Fig. 3. Time-varied CA1 interneuron response to CNO injection. (*A*, *Top*) *Z*-scored firing rate (calculated in 60-s windows at 30-s steps) of all seven interneurons from a single session (subject 7, session 2). Note that some interneurons increase their firing rate while others are silenced. Unit numbers are indicated in the legend. (*A*, *Bottom*) State scoring for this session with states indicated in the legend. (*B*) Interneuron auto- and cross-correlograms from selected epochs. In this case, three wake epochs were chosen (shaded in gray, labeled with lowercase letters). Epoch *a*, baseline, before injection of CNO + DMSO. Epochs *b* and *c*, approximately 1 and 2 h after injection. Note the altered cross-correlations between neuron pairs following drug injection. (*C*) Histograms quantifying return to baseline after injection of CNO + DMSO for the above session. Proportion of time following injection during which each cell firing rate was >20% of baseline firing rate (*Top*) and >100% of baseline FR is plotted. Pyramidal cells (*Left*) reliably spend very little time in recovery following CNO + DMSO injection. Interneurons (*Right*) reflect a mixed picture, with some spending varying epochs above, and others below, baseline.

longer-term (tens of minutes to hours) changes were also reflected by the short-term (±50 ms) cross-correlograms between interneuron pairs. Spikes of interneuron pairs with a positive correlation at the theta timescale during baseline recording could become negatively correlated for extended time periods under CNO (Fig. 3*B*) or vice versa (*SI Appendix*, Fig. S3). To quantify the within-session variability of firing patterns, we determined the mean firing rates of the pyramidal cells and interneurons in 60-s-long successive time windows after CNO injection and calculated the fraction of time windows with ≥20 to 100% (suppression) and >100% (facilitation) of the baseline firing rate. As expected, pyramidal neurons only exceptionally exceeded the baseline firing rates in any time window and, in fact, in the majority of post-CNO time windows had firing rates less than 20% of their baseline rates (Fig. 3*C*). Although several interneurons exceeded their baseline spiking (100%) transiently in many time epochs, the majority of interneurons typically fired below baseline. In many epochs, interneurons did not even exceed 20% of their baseline rates (Fig. 3*C* and *SI Appendix*, Fig. S4).

We hypothesized that heterogeneous strengths of inhibitory connectivity among interneurons can explain why a small group of transiently active neurons can exert a strong inhibition on the majority and counter the direct effect of homogeneous CNO stimulation of all interneurons. To test this hypothesis, we constructed a population model from leaky integrate-and-fire pyramidal cells (n = 4,000) and interneurons (n = 1,000; *SI Appendix*, Fig. S5*A*) (24). The firing rate distribution across model neuron groups was adjusted to match those of the recorded neurons (*SI Appendix*, Fig. S4 *B–D*). After a control period during which both pyramidal cells and interneurons received noise stimulation, we added tonic excitation to the interneuron population, mimicking the effect of CNO in vivo. Even though all interneurons received a steady excitatory boost uniformly, the overall firing rates of both interneurons and pyramidal cells decreased (*SI Appendix*, Fig. S5 *B–D*), similar to the in vivo situation. The stronger the CNO activation, the stronger the suppression of firing rates of both interneurons and pyramidal cells (*SI Appendix*, Fig. S5*E*). The reason for this paradoxical effect could be explained by the elevated firing of a minority, which suppressed the activity of other interneurons and the pyramidal cell population. Since the simulated interneurons were of the same type with similar biophysical properties, the overall distribution of firing rate changes after "CNO activation" can be explained only by the synaptic connectivity strength differences among the interneurons. As a result, the nature of the interaction between interneurons and pyramidal cells also changed (*SI Appendix*, Fig. S5 *F* and *G*).

Effect of Interneuron-Mediated Suppression of CA1 Pyramidal Cells on the LFP. The CNO-induced large firing rate decrease of pyramidal cells did not bring about visually striking effects on the LFP (Fig. 1 *B–D*). Spectral analysis of the LFP patterns revealed that CNO administration decreased LFP power progressively more effectively from 20 to 400 Hz. This effect was prominent in both waking (immobility and walking) and sleep (non-REM and REM; Fig. 4*A*). The smallest effect was seen in the theta (6 to 9 Hz) band, while the most prominent difference occurred in the sharp wave ripple band (SPW-R; 110 to 160 Hz; Fig. 4*A* and *SI Appendix*, Fig. S6). Since spikes and spike afterpotentials contribute to the LFP down to 40 Hz (22, 25, 26), at least part of the power decrease at higher frequencies could be explained by the decreased spiking frequency of the majority pyramidal neurons.

During ambulation with regular theta oscillations, we examined the theta phase preference of neuronal spikes because theta

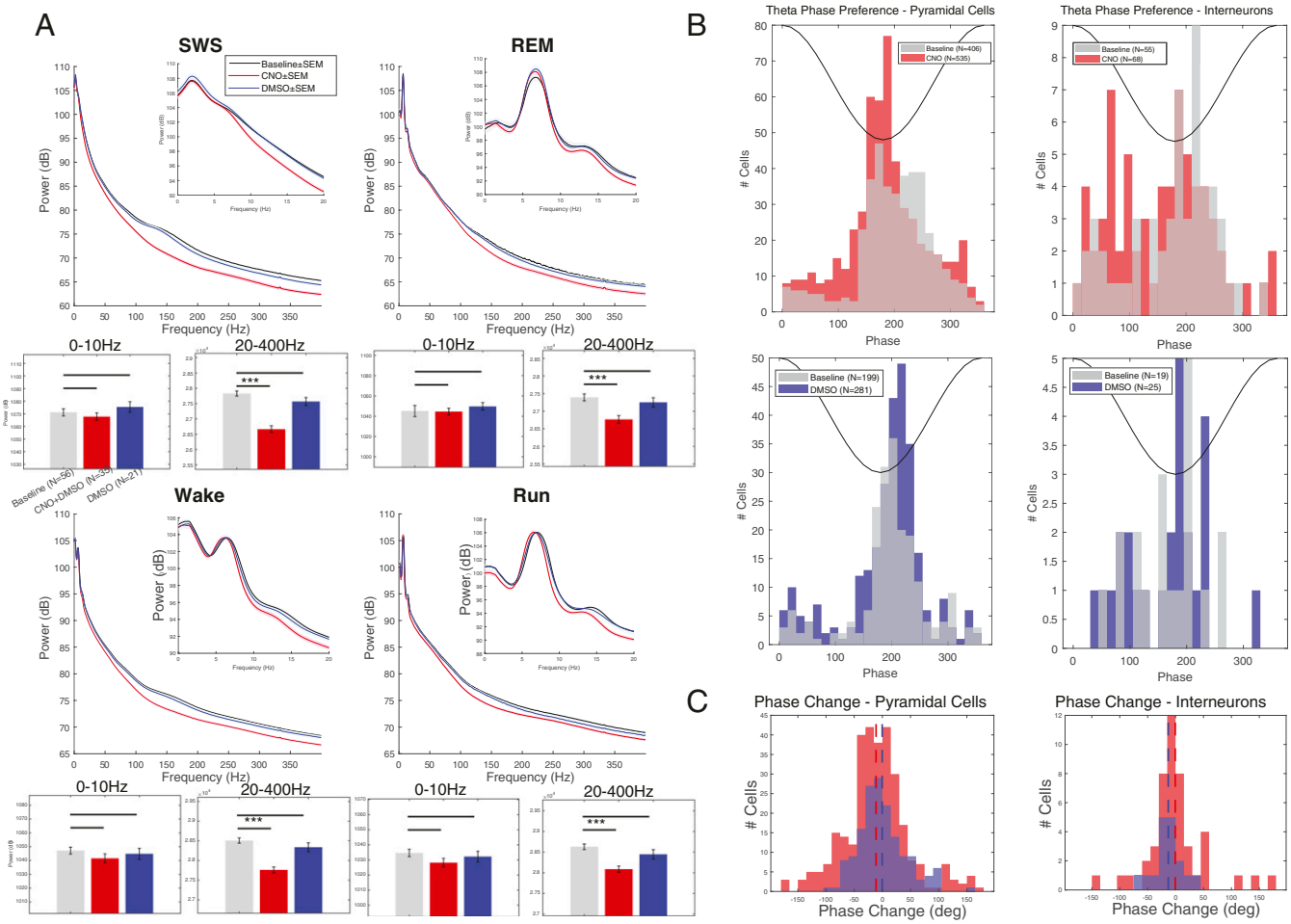

Fig. 4. LFP changes after CNO administration. (*A*) Average state-specific power spectra over 0 to 400 Hz and 0 to 20 Hz (*Insets*) at baseline (gray) and after injection of CNO + DMSO (red) or DMSO only (blue) for all rats. Sessions were state-scored to identify slow-wave sleep (SWS), REM sleep, wake, and run states. Note the relative decrease of high-frequency power after CNO + DMSO injection in each state. Averaged band power for 0 to 10 Hz and 20 to 400 Hz is shown in the bar graphs for each state. Power after CNO injection was significantly affected only for the 20- to 400-Hz band in each state. (*B*) Distribution of spike theta phase preference (in degrees) for individual pyramidal cells (*Left*) and interneurons (*Right*) at baseline (gray) and after injection of CNO + DMSO (*Top*; red) or DMSO only (*Bottom*; blue). (*C*, *Left*) Change in spike theta phase for pyramidal cells with a significant phase preference in both baseline and injection epochs for CNO + DMSO (red) and DMSO only (blue). The difference in phase change was significant (−11.1° in CNO + DMSO vs. −0.33° in DMSO, $P = 0.04$). Means are indicated with dotted vertical lines. (*C*, *Right*) Same display for interneurons. The difference in phase change was not significant (−13.2° in CNO + DMSO vs. −0.65° in DMSO, $P = 0.36$). Means are indicated with dotted vertical lines. ***$P < 0.0005$.

phase assignment of pyramidal cell spikes is precisely regulated by the temporal constellation of a variety of interneuron spikes (27, 28). As a result of chemogenetic perturbation of interneurons, the preferred phase of pyramidal cell spikes shifted forward to earlier phases (i.e., to the trough) after CNO but not after vehicle administration (Fig. 4 *B* and *C*). This may be explained by the reduced efficacy of the time (i.e., theta phase) control of perisomatic inhibition (28).

Population Bursts Persist during DREADD-Induced Suppression of CA1 Pyramidal Cells. Although CNO strongly suppressed the overall firing rates, the population bursts of pyramidal cells and corresponding SPW-Rs persisted (Fig. 5). To allow for a more consistent assessment of these changes, SPW-R features were computed only during non-REM sleep episodes, and separately for sharp waves in the stratum (str.) radiatum and ripples in the pyramidal layer. Ripple rate was expressed as the number of detected ripples with peak envelop power >5 SD of the baseline (29). The incidence of such magnitude-thresholded ripples was reduced twofold across all animals and the reduction was consistent in each rat (Fig. 5 *A* and *B* and *SI Appendix*, Fig. S7). The amplitude and, to a small extent, duration of the persisting ripples under CNO were also reduced, while ripple frequency was not affected (Fig. 5 *C*–*E* and *SI Appendix*, Fig. S7).

In two rats, with a linear silicon probe placed in the CA1–dentate gyrus axis, we were able to monitor the current sink and source changes of SPWs and ripples. The depth profile of CA1 ripple and sharp wave remained unaltered by CNO injection (Fig. 6*A*) but the magnitudes of both the ripple source in the CA1 pyramidal layer and the sharp wave sink in the str. radiatum were reduced. To assess this relationship quantitatively in all animals with multishank probes, we visually inspected the distribution of LFP from each recording site in each animal. Since some recording sites of the multiple-shank electrodes were below the pyramidal layer in several sessions, we regarded the negative waves recorded from these electrode sites as a proxy for sharp wave (30). The voltage difference between the site with the largest negative LFP deflection and an electrode in the pyramidal layer with a positive SPW was used to quantify the amplitude of SPWs and detect their incidence. Sharp wave incidence after CNO injection decreased but it reached significance in only two of the eight rats (Fig. 5*B*). The amplitude of

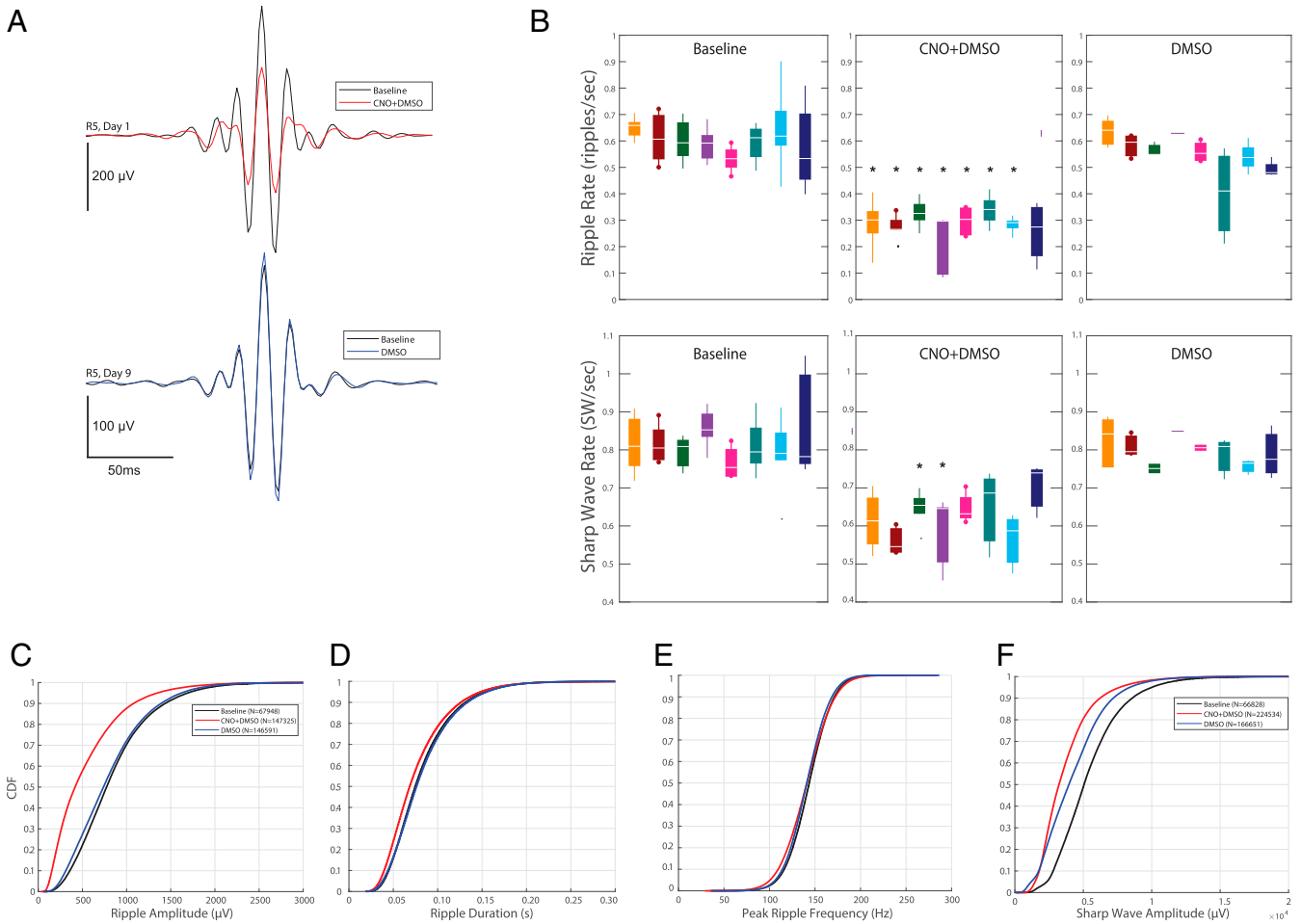

Fig. 5. Effect of CNO on features of sharp wave ripples. (*A*) Ripple peak-triggered average LFP before (black) and after CNO (red) in the CNO session (*Top*) and DMSO vehicle session (*Bottom*) in the same rat (R5). The CNO and DMSO injections were given on different days. (*B*, *Top*) Ripple rate for each rat ($n = 8$; color-coded for each rat) at baseline (*Left*) and after injection of CNO + DMSO (*Middle*) or DMSO only (*Right*). Asterisks indicate statistically significant differences from baseline after a Bonferroni correction ($\alpha = 0.05$/number of comparisons). Rats 2 and 5 (dots on whiskers) had CA1-dentate gyrus-spanning linear silicon probes. (*B*, *Bottom*) Same as above but for sharp waves detected independent of ripples. (*C*) Empirical cumulative distribution function (CDF) for ripple amplitude for all detected SWR complexes (indicated by *N* in legend) in all sessions at baseline (black) and after injection of CNO + DMSO (red) or DMSO only (blue). (*D–F*) Same display as in *C* for ripple duration, peak ripple frequency, and sharp wave amplitude. Refer to *SI Appendix* for details of calculations of these metrics. Rates are calculated as number of ripples or sharp waves per second non-REM time.

the sharp wave also decreased significantly (*SI Appendix*, Fig. S7). In DMSO vehicle sessions, the quantitative aspects of both sharp waves and ripples remained unaltered (Fig. 5 and *SI Appendix*, Fig. S7).

The positive correlation between the negative sharp wave amplitude and ripple amplitude (30) was not only preserved but enhanced after CNO administration (Fig. 6*B*), that is, a similar amplitude sharp wave coincided with a larger ripple amplitude than prior to CNO injection or the control DMSO session. Many sharp waves failed to induce a ripple, potentially indicating that population bursts in CA3, which give rise to the sharp wave sink in the str. radiatum, were not always effective in inducing ripples in CA1. To quantify such failures, we calculated the ratio of paired to unpaired sharp waves in each condition. "Paired" sharp waves had a concurrently detected ripple in the pyramidal layer, whereas "unpaired" sharp waves did not. The ratio of paired vs. unpaired sharp waves decreased significantly after CNO injection (Fig. 6*C*), showing that while the CA3 region continued to produce population bursts and associated depolarization of the CA1 population (as reflected by the sharp wave), not all of them succeeded in inducing a ripple event and the failures were accentuated under the effect of CNO.

Although the incidence of SPW-Rs decreased and tonic spiking activity of pyramidal neurons markedly decreased after CNO administration, spike coupling to SPW-R in the surviving events was, unexpectedly, stronger (Fig. 7 *A–C*). This was reflected by comparing the normalized probability of firing between −50 and +50 ms of SPW-R peaks before and after drug administration (pyramidal cells in CNO sessions: control 0.46, CNO 0.57, $P = 5.4669e\text{-}65$; $n = 716$; pyramidal cells in DMSO sessions: control 0.49, DMSO 0.487, $P = 0.548$; $n = 306$; interneurons in CNO sessions: control 0.38, CNO 0.42, $P = 0.139$; $n = 48$; interneurons in DMSO sessions: control 0.45, DMSO 0.45, $P = 0.794$; $n = 22$). In effect, CNO produced a larger excitatory gain during surviving SPW-Rs compared with drug-free control epochs. These population burst changes were not brought about by a uniform firing rate shift of individual interneurons. Instead, a variety of different firing pattern alternations were observed, including no change, increased ripple-related recruitment, ripple-related decrease, or timing differences of interneurons (Fig. 7*D*). The spike coupling of both pyramidal cells and interneurons to SPW-Rs was unaffected by DMSO vehicle injection (Fig. 7).

Overall, these findings demonstrate that while CNO activation of interneurons in the CA1 hippocampal region brings about a

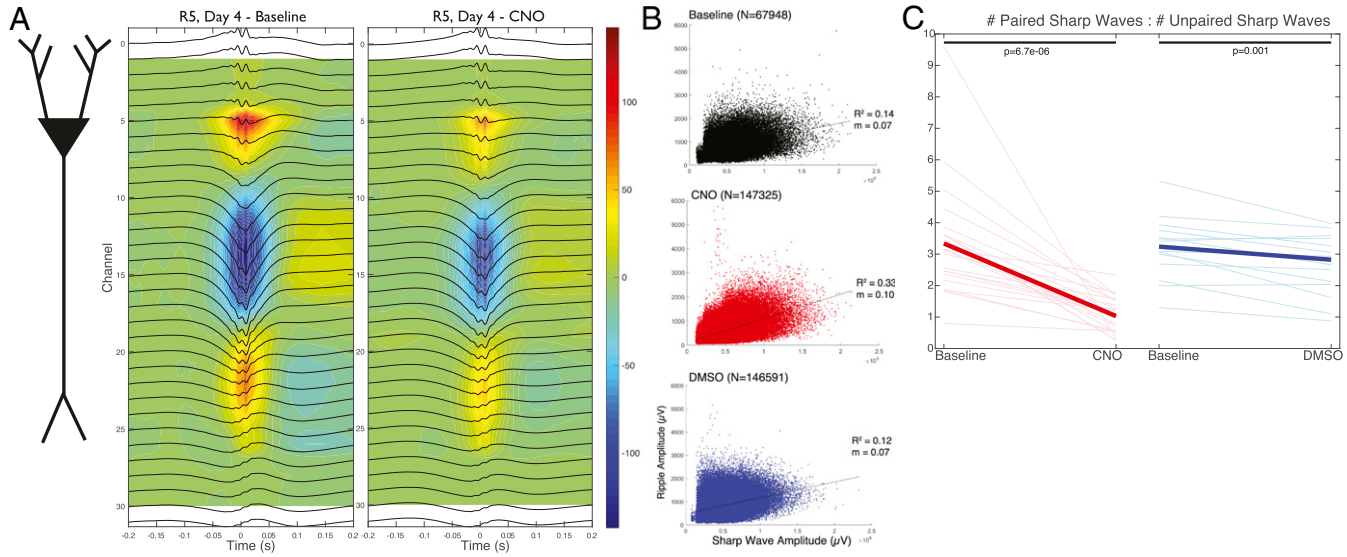

Fig. 6. Effects of CNO on sharp waves and ripples. (*A*, *Left*) Schematic of a pyramidal cell extending through the layers of CA1. (*A*, *Middle*) Ripple peak-triggered average current source density (CSD) map in a baseline epoch for a representative baseline session. Ripple-triggered average LFPs at each recording site are superimposed. Sources are represented in blue and sinks in red. (*A*, *Right*) Ripple-triggered average CSD in a CNO + DMSO session of the same rat. (*B*) Peak ripple amplitudes versus sharp wave amplitudes for paired SPW-Rs. Sharp waves were detected as a difference of traces from the str. radiatum and str. pyramidale. Plotted values correspond to all baseline SPW-R complexes (*Top*; black), all post–CNO + DMSO SPW-R complexes (*Middle*; red), and all post–DMSO-only SPW-R complexes (*Bottom*; blue). Best linear fits are displayed with corresponding slope (*m*) and R^2 values. Note that similar sharp wave amplitudes correspond to larger ripple amplitudes after injection of CNO (larger *m*). (*C*) Ratio of paired to unpaired sharp waves at baseline and after injection of CNO + DMSO (individual pink lines) or DMSO only (individual light blue lines). Mean values are shown (thick red, thick blue lines). Paired sharp waves are a subset of those sharp waves, detected in the str. radiatum, which do not have a concurrently detected ripple in the pyramidal layer. Unpaired sharp waves are the remaining ones (i.e., those without a detected ripple).

strong and long-lasting suppression of baseline firing rates of pyramidal cells and decreases the incidence of SPW-Rs, population burst activity during the surviving SPW-Rs is paradoxically increased.

Long-Term Plasticity of CNO-Induced Changes. In addition to altering the short-term temporal dynamics of interneurons and pyramidal cells, CNO injection also brought about long-term changes (Fig. 8). After CNO injection, the firing rates of neurons did not return back to baseline within the recording session (up to 12 h; *SI Appendix*, Fig. S8*A*), yet recovery was complete within 24 h. This was demonstrated by comparing the daily pre-CNO epochs (*SI Appendix*, Fig. S8 *B* and *C*). Although the identity of the recorded neuronal populations changed in subsequent sessions, due to small movement of the electrode after each session, the population firing rates of both pyramidal cells and interneurons were remarkably similar during pre-CNO control epochs over days.

The recovery of predrug baseline firing in control conditions from day to day does not imply that the impact of CNO-induced effects remained the same over days (Fig. 8*A*). By calculating the fraction of 60-s time windows pyramidal neurons fired above 20% of the baseline firing rate during post-CNO epochs (as in Fig. 3*B*), we found that the same dose of CNO had a markedly weaker effect on the second and subsequent CNO sessions, compared with the first one (Fig. 8 *A* and *B*). In contrast, the firing rates of interneurons did not change significantly over days (Fig. 8*B*). These findings indicate that while CNO exerted the same activation effect on interneurons each day, the interneuron-to-pyramidal neuron inhibitory synapses underwent long-term change.

Discussion

We examined the physiological changes in the CA1 region of the hippocampus in response to pharmacogenetic activation of all inhibitory interneuron types. The firing rate of CA1 pyramidal cells was strongly decreased for several hours but the duration and magnitude of suppression were attenuated after repeated daily injection of the DREADD activator CNO. Unexpectedly, the population firing rate of interneurons did not increase after CNO administration and only a small fraction of interneurons showed sustained elevated firing activity. Instead, interneurons alternated between low- and high-firing rate epochs over time. The power of low-frequency LFP remained largely unchanged. While the incidence of SPW-Rs decreased, the surviving population bursts were stronger compared with the vehicle control condition. Thus, DREADD activation of interneurons does not bring about continual silencing of principal cells but, instead, a nonuniform suppression with strong intermittent population bursts.

DREADD-Induced Nonuniform Activity Changes. DREADD methods have been introduced with the intention of producing predictable perturbation of genetically identified neuron classes sustained over long time periods (1–4). Activation and inactivation of neurons are typically performed to study gain of function and loss of function in particular classes of neuron types. The induced physiological or behavioral changes are then interpreted as the contribution of that neuron type. However, interpretation of the outcome of perturbation in networks with feedback and nonlinear gain is not straightforward. Computational and optogenetic studies have already alerted to the problem of nonspecificity in terms of the perturbation outcome (11, 31, 32). For example, optogenetic activation of CaMKII neurons is tacitly expected to bring about uniform enhancement of pyramidal cell discharge. However, oftentimes a sizable portion of the CaMKII-expressing neurons is suppressed via recruitment of local inhibition (7–9).

In our experiments, CNO is expected to activate all interneuron types (15). Yet, spiking of interneurons as a population did not uniformly increase but, instead, CNO perturbed the inhibition-stabilized CA1 circuit (33–36) and led to a decreased

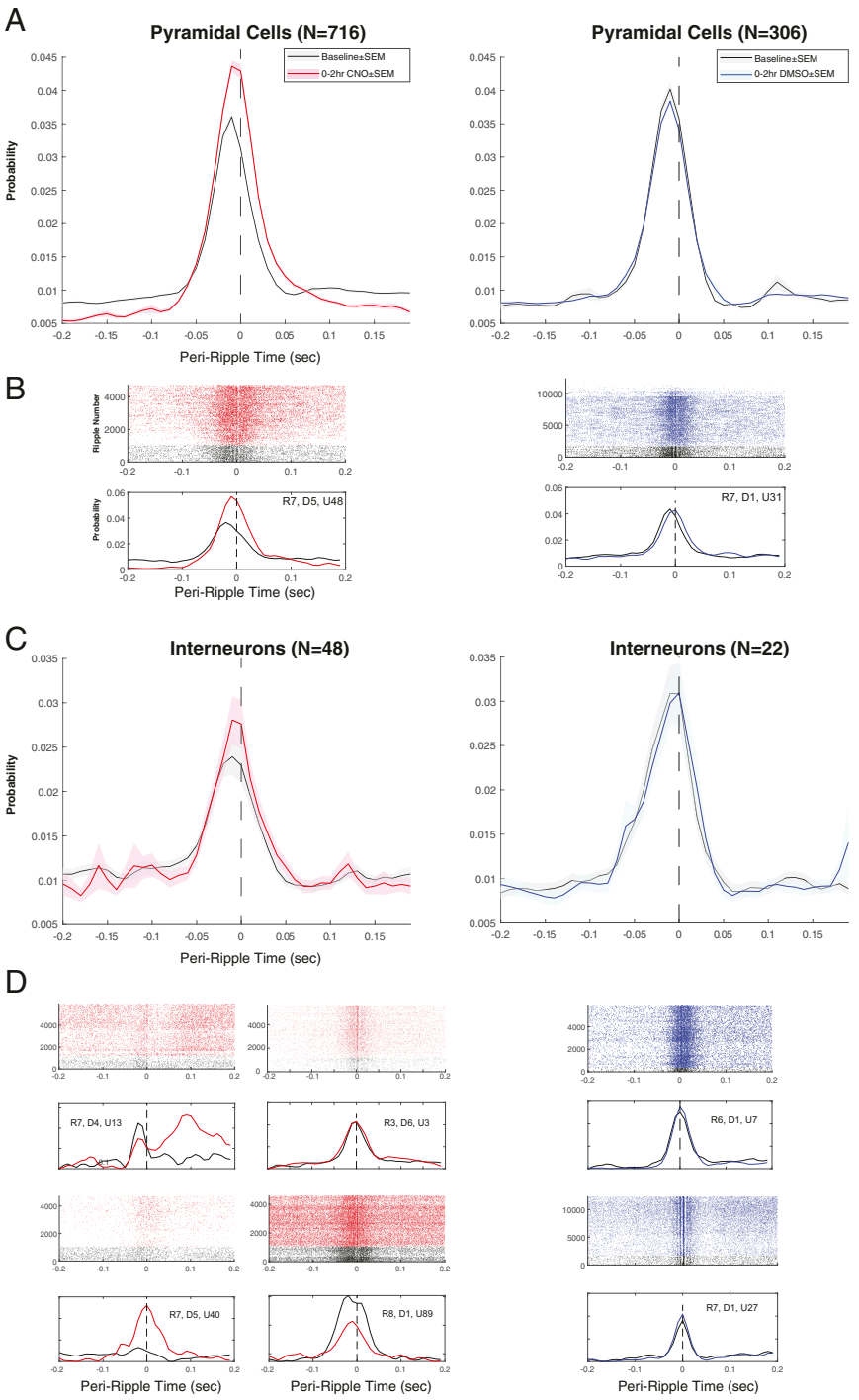

Fig. 7. Persisting SPW-Rs after CNO are more synchronous. (*A*) Average peri-ripple time histogram for pyramidal cells at baseline (black line; ±SEM) and for the first 2 h after injection of CNO + DMSO (*Left*; red line; ±SEM) or DMSO only (*Right*; blue line; ±SEM). Note the increased probability of firing during the SPW-R after CNO + DMSO. (*B*, *Top*) Ripple-triggered raster plot of spike times for a single representative pyramidal cell at baseline (black) and after injection of CNO + DMSO (*Left*; red; rat 7, day 5, unit ID 48) or DMSO only (*Right*; blue; rat 7, day 1, unit ID 31). (*B*, *Bottom*) Peri-ripple time histogram corresponding to baseline (black) and the first 2 h after injection (red or blue) for the same units as above. (*C*) Average peri-ripple time histogram for interneurons at baseline (black line; ±SEM) and for the first 2 h after injection of CNO + DMSO (*Left*; red line; ±SEM) or DMSO only (*Right*; blue line; ±SEM). (*D*) Ripple-triggered raster plot of spike times for representative interneurons at baseline (black) and after injection of CNO + DMSO (red) or DMSO only (blue). Below each raster plot are corresponding peri-ripple time histograms at baseline (black) and the first 2 h after injection (red or blue).

firing in many interneurons (10, 11). Only a few neurons showed consistent and relatively sustained firing rate elevation. The majority of interneurons increased and decreased their rates in an intermittent and interleaved manner. Thus, the several-fold decrease of pyramidal cell discharge was brought about by continually changing subpopulations of interneurons with transient high firing rates. Although their local excitation was largely eliminated by the silent CA1 pyramidal neurons, they still received

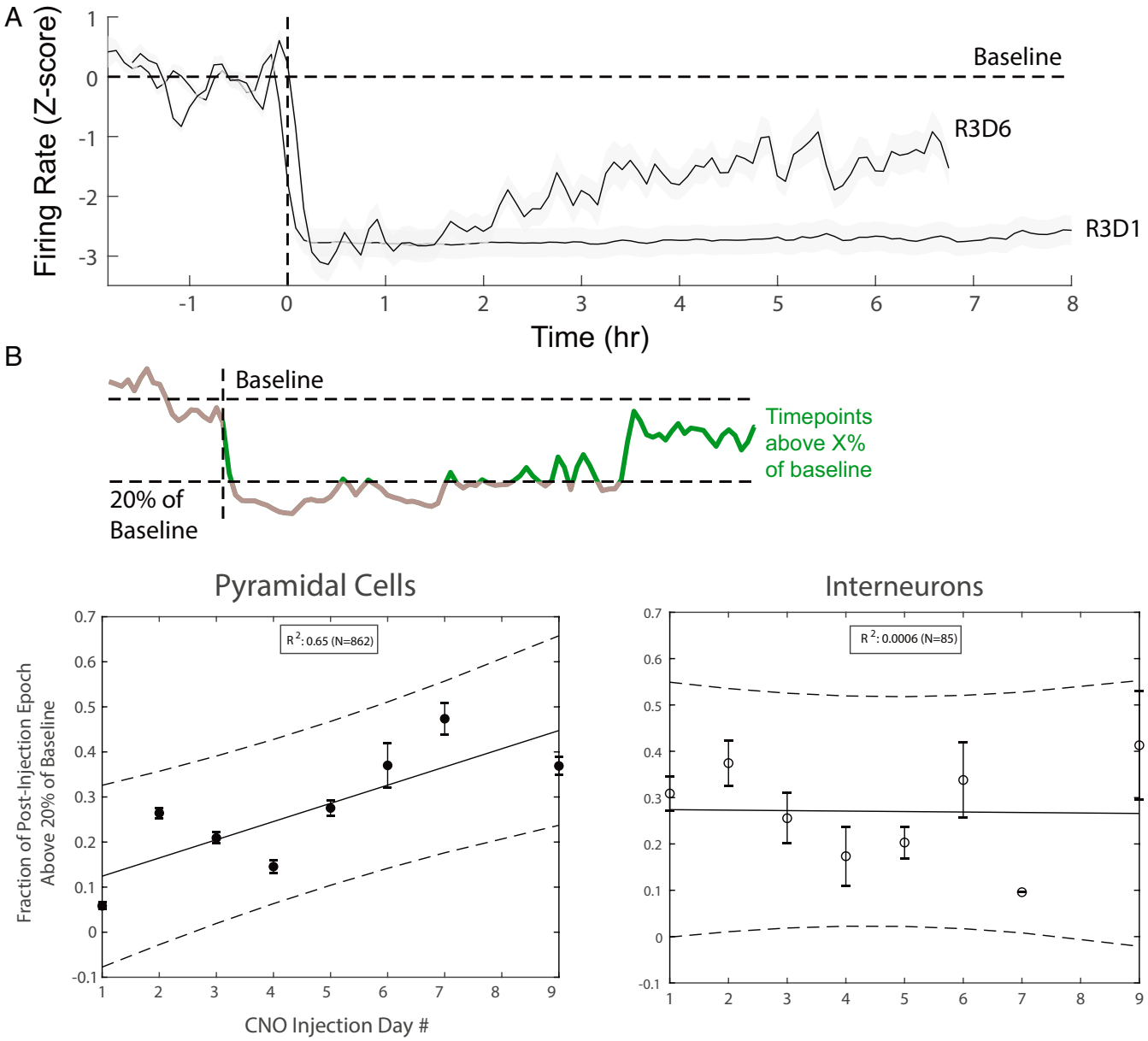

Fig. 8. Long-term plasticity induced by CNO administration. (*A*) Population firing rates of pyramidal neurons before and after CNO injection on the first day and sixth day of CNO exposure in a single rat (R3). Firing rates were time-averaged in 600-s windows (300-s steps) and *Z*-scored, and then averaged across all pyramidal cells for a given session. (*B*, *Top*) Schematic demonstrating quantification of cell firing rate recovery. Baseline is determined using the preinjection epoch (to the left of the dashed line), and a threshold (20%) is set above which time points are said to have begun to return to baseline (green). Time points below this threshold (gray) are not included. An overall fraction of time (maximum 4 h) spent above threshold is calculated for each cell. (*B*, *Bottom*) Distribution of the above fractions for pyramidal cells (*Left*) and interneurons (*Right*). Linear regression was performed for each plot, with a strong positive correlation with CNO injection day for pyramidal cells and no correlation for interneurons.

feedforward inputs from CA3 pyramidal cells and entorhinal cortex and subcortical sources (37). In principle, the variable firing patterns of interneurons could be explained by these upstream afferents. However, under this hypothesis, one might expect that the majority of interneurons would fire in a temporally coordinated manner and change predictably with brain state changes. However, this is not what we observed even within the same brain state.

In addition to physiological phasic activation from extra-CA1 inputs, interneurons also received artificial steady-state excitation by CNO. It is possible that some interneuron "types" (10, 27) were more effectively excited than others, although it is not known whether some interneuron types express the Dlx5/6 genes differentially (14) or whether they have differential affinity to CNO. Another possible source of the variability is the nonuniform connectivity of different interneuron types (10, 27, 38) so that one or a few types of interneurons were excessively active and, in turn, suppressed both pyramidal cells and the remaining interneurons. Finally, it is important to emphasize that even if all interneurons were uniformly activated and randomly connected, they are not expected to sustain tonically increased rates as our computer model of interneuron networks illustrated. Both in the experiment and in the model, the total number of interneuron spikes decreased per unit time. Thus, it is unlikely that the superactivity of a small subgroup of interneurons was responsible for the depression of firing rates of both the pyramidal and interneuron populations. Instead, it is more likely that the uniform

activation of interneurons by CNO suppressed the activity of pyramidal cells and thus disfacilitation was an important factor in the decreased overall interneuron firing. On the other hand, the heterogeneity of the interneuron firing rates can be explained by their preexisting difference in synaptic connectivity.

We suggest further that the waxing and waning pattern of neuronal firing of interneurons was due to the depressing nature of interneuron–interneuron and interneuron–pyramidal neuron synapses (39, 40), so that a fraction of interneurons can become transiently active and, when their suppressing impact on other interneurons wanes, a new population becomes active, as predicted by theoretical considerations (10, 11). Our findings and modeling results are best compatible with this last scenario, given that we did not find differences in waveform features, baseline firing rate and burst index parameters, or relationship to SPW-Rs. Further experiments, targeting homogeneous subpopulations, will elucidate whether the temporal dynamics observed here were brought about by a small minority of active neurons with widespread connectivity or whether even within a homogeneous interneuron group interleaved activity is the norm.

Differential Impact of DREADD Activation on the LFP. Despite the large reduction of firing rates of the pyramidal cell population after CNO injection, the impact on low-frequency LFP was relatively minor, especially in the theta band. This finding illustrates that the major transmembrane currents that give rise to the extracellular LFP arise largely from the excitatory postsynaptic currents brought about by the afferent inputs to CA1 and the inhibitory postsynaptic currents (IPSCs) induced by the relatively unchanged overall activity of interneurons (25).

In contrast to lower frequencies, faster bands were attenuated in all brain states. More efficient volume conduction of extracellular fields in the lower-frequency bands may be one possible mechanism of this differential effect. A major source of gamma-frequency oscillations is the IPSCs brought about by pyramidal–basket interneuron interactions (41, 42). Since pyramidal neurons were less active under the effect of CNO, their temporal coordinating effect on perisomatic basket neurons also decreased. In turn, the synchrony of IPSCs on pyramidal neurons was attenuated. Such change may explain at least part of the power decrease of high-frequency LFP. In addition to attenuated gamma oscillations, the reduced number of pyramidal neuron spikes also contributed to the decreased power, especially in the "high-gamma" (>150 Hz) band. Spikes and especially spike afterpotentials are known to contribute to high-frequency power and their impact is detectable down to 40 Hz (25, 22, 26).

Effect of DREADD Activation on SPW-R–Associated Population Bursts. The SPW-R complex has two independent components. The sink of sharp wave in the str. radiatum reflects the inward current brought about by a convergence population burst from the CA2 and 3 regions. Sharp waves are most often coupled by an induced ripple event in the CA1 pyramidal layer (30). Since our DREADD manipulations targeted the CA1 region, we expected a dissociation between the two events. Indeed, we found that both the incidence and, to a moderate degree, the amplitude and duration of ripples decreased. After CNO, but not vehicle, injection, a large fraction of sharp waves detected in the str. radiatum were no longer associated with a ripple in the pyramidal layer ("uncoupled" sharp waves).

During sharp waves that were coupled to ripples, the sink in the str. radiatum under CNO was weaker compared with the control and DMSO vehicle conditions. One explanation for the decreased str. radiatum sink is the reduced perisomatic inhibition (an active source) and the consequently reduced passive return current in the str. radiatum (30). Alternatively, the reduced sink in the str. radiatum may be interpreted as decreased excitation of CA1 pyramidal neurons by their sharp wave-inducing CA2 and 3 inputs. Although no virus-infected neurons were observed in the CA2 and 3 regions, the minimal infection of interneurons in the dentate gyrus/hilus region can serve as a potential explanation. The activation of dentate gyrus/hilus interneurons may also explain the reduced incidence of sharp waves during the CNO effect, although reduction of sharp wave incidence was much less affected than that of ripples. Overall, these findings are compatible with the explanation that the CA2/3-induced population bursts continued to excite CA1 pyramidal neurons, as reflected by the LFP sharp waves, yet such bursts often failed to give rise to a ripple oscillation in the CA1 circuit.

Unexpectedly, and in contrast to the striking suppression of "background" firing of pyramidal neurons, half of the SPW-Rs persisted after CNO injection. Moreover, population bursts of pyramidal cells were stronger in the surviving sharp waves and sharp waves of the same magnitude were coupled with large-amplitude ripples. The pyramidal spike composition of population effects also varied. These findings support a hypothesis that the physiological mechanisms responsible for inhibiting individual pyramidal cell spikes and synchronous population bursts are different (28). While SPW-Rs are associated with increased recruitment of both pyramidal cells and interneurons, pyramidal cell recruitment exceeds the recruitment of the interneurons by a factor of 2 to 3, yielding a large excitatory gain (29). This gain is explained by the strong pyramidal cell–interneuron synapse and the large synchrony of neurons during SPW-Rs. Because a single pyramidal cell spike can induce a spike in its target interneuron (43), other pyramidal neurons firing within 1 to 2 ms cannot recruit further spikes in the same interneuron (29). The CNO-induced impaired coordination of interneurons may explain why doses of CNO which can bring about complete suppression of spiking in individual pyramidal neurons still fail to suppress population bursts.

Ripple frequency remained unchanged, despite the reorganization of interneuron interactions. Ripple frequency is remarkably constant in the same brain state. During development, SPWs are present at birth and the magnitude of SPW burst increases several-fold but ripples begin to emerge only at the end of the second postnatal week. Once ripples emerge, the intra-ripple frequency assumes adult values (44). Ripple frequency is believed to be determined by the $GABA_A$ receptor time decay at synapses between parvalbumin-expressing basket neurons (45) and by voltage-gated Na^+ channels in the dendrites of basket cells (46).

An important practical implication of our findings is that DREADD-induced physiological changes may not always bring about the desired switch-off or switch-on effects because of the immediate and effective reorganization of the escaping minority of neurons. In the case of the hippocampal CA1 region, the behavioral interpretation of DREADD-induced background silencing should also consider the impact of the remaining population bursts in the form of SPW-Rs.

DREADD-Induced Long-Term Plasticity. Repeated DREADD manipulations are often used to probe behavior under the tacit assumption that daily application of the ligand activator will exert similar effects (5, 16–21). Our observations indicate that this may not be the case. While suppression of pyramidal neurons was prominent on each day of CNO administration, the drug's efficacy was reduced upon repeated injections. At least two possible targets can account for this long-term plastic effect. First, the CNO target receptor in interneurons may be plastic. However, the observed stability of the interneuron responses over days argues against this possibility. We acknowledge though that a potential heterogeneity of CNO affinity in different types of interneurons cannot be fully excluded. If long-term plasticity took place in a small but specific subset of interneuron types, our

sampling of relatively low numbers of unidentified interneurons in each session would not be able to detect it. The second potential site of plasticity is the interneuron–pyramidal cell synapse. Our findings favor this interpretation. Both short-term and long-term plasticity have been demonstrated between inhibitory neurons and pyramidal cells and among inhibitory interneurons (40, 47, 48).

The long-term (~24 h) attenuation of the CNO-induced suppressive effect on pyramidal neurons stands in sharp contrast to the stability of the firing rate population during the daily pre-CNO control epochs. In other words, the effect of the previous day's CNO was completely washed out when judged from the baseline spontaneous firing rates of neurons yet was clearly present when tested during post-CNO epochs. A potential mechanism for such a drug-dependent effect is long-term potentiation of the short-term suppression by interneurons, usually referred to as metaplasticity (49). Under this hypothesis, physiological levels of activity of interneurons would keep the inhibitory–excitatory balance within boundaries during the pre-CNO control epochs. However, when interneuron activity is transiently enhanced, as was observed during CNO exposure, the altered short-term suppression would inhibit pyramidal neurons less effectively after repeated CNO injections (50). Confirming this hypothesis will require directly monitoring the efficacy of inhibitory synapses upon repeated activation of various interneuron types. Overall, these findings illustrate how long-term effects of neuronal circuits are brought about by repeated use (51–56).

In conclusion, DREADD activation may bring about unexpected paradoxical effects, such as parallel decrease of population firing rates of both interneurons and pyramidal cells, differential effects on background activity and population bursts, and induction of plasticity in the affected circuits. These changes, therefore, should be considered in the application of the DREADD method and its impact on circuit function and behavior. Our findings likely generalize to cortical regions and other manipulations, such as traditional pharmacological and optogenetic activation of interneuron populations.

Materials and Methods

All experiments were approved by the Institutional Animal Care and Use Committee at New York University Langone Medical Center (NYULMC). pAAV-hDlx-Gq-DREADD-dTomato-Fishell-5 was infused into the hippocampal CA1 region in rats to express excitatory DREADD (hM3Dq) in all interneurons and 2 wk later implanted with silicon probes. After baseline control recording, the animals received an intraperitoneal injection of either 5 mg/kg CNO to activate interneurons or DMSO (vehicle control). Recorded neurons were separated into putative pyramidal cells and interneurons. Details of surgery, physiological recordings, and data analyses are presented in *SI Appendix*.

Data Availability. The processed and wideband data reported in this article have been deposited in the Buzsaki Lab Databank, https://buzsakilab.com/wp/public-data/, and are also available at http://doi.org/10.5281/zenodo.4307883 per PNAS policy.

ACKNOWLEDGMENTS. We thank Gord Fishell, Jennifer Gelinas, and Dion Khodagholy for initiating these experiments, and Thomas Hainmueller and Yiyao Wang for comments on the manuscript. Supported by a European Molecular Biology Organization (EMBO) postdoctoral fellowship (EMBO ALTF 1161-2017 to M.V.), a Human Frontiers Science Program postdoctoral fellowship (LT0000717/2018 to M.V.), the Department of Neurosurgery and Office of Graduate Medical Education at NYU Langone Health (P.R.), and NIH Grants MH122391, MH107396, U19 NS107616, and U19 NS104590.

1. B. N. Armbruster, X. Li, M. H. Pausch, S. Herlitze, B. L. Roth, Evolving the lock to fit the key to create a family of G protein-coupled receptors potently activated by an inert ligand. *Proc. Natl. Acad. Sci. U.S.A.* **104**, 5163–5168 (2007).
2. J. G. English, B. L. Roth, Chemogenetics—A transformational and translational platform. *JAMA Neurol.* **72**, 1361–1366 (2015).
3. D. J. Urban, B. L. Roth, DREADDs (designer receptors exclusively activated by designer drugs): Chemogenetic tools with therapeutic utility. *Annu. Rev. Pharmacol. Toxicol.* **55**, 399–417 (2015).
4. J. L. Gomez *et al.*, Chemogenetics revealed: DREADD occupancy and activation via converted clozapine. *Science* **357**, 503–507 (2017).
5. D. F. Manvich *et al.*, The DREADD agonist clozapine N-oxide (CNO) is reverse-metabolized to clozapine and produces clozapine-like interoceptive stimulus effects in rats and mice. *Sci. Rep.* **8**, 3840 (2018).
6. C. J. Magnus *et al.*, Ultrapotent chemogenetics for research and potential clinical applications. *Science* **364**, eaav5282 (2019).
7. E. Stark, T. Koos, G. Buzsáki, Diode probes for spatiotemporal optical control of multiple neurons in freely moving animals. *J. Neurophysiol.* **108**, 349–363 (2012).
8. S. Trouche *et al.*, Recoding a cocaine-place memory engram to a neutral engram in the hippocampus. *Nat. Neurosci.* **19**, 564–567 (2016).
9. I. Gridchyn, P. Schoenenberger, J. O'Neill, J. Csicsvari, Assembly-specific disruption of hippocampal replay leads to selective memory deficit. *Neuron* **106**, 291–300.e6 (2020).
10. T. F. Freund, G. Buzsáki, Interneurons of the hippocampus. *Hippocampus* **6**, 347–470 (1996).
11. M. V. Tsodyks, W. E. Skaggs, T. J. Sejnowski, B. L. McNaughton, Paradoxical effects of external modulation of inhibitory interneurons. *J. Neurosci.* **17**, 4382–4388 (1997).
12. G. Turrigiano, Too many cooks? Intrinsic and synaptic homeostatic mechanisms in cortical circuit refinement. *Annu. Rev. Neurosci.* **34**, 89–103 (2011).
13. A. Mitra, S. S. Mitra, R. W. Tsien, Heterogeneous reallocation of presynaptic efficacy in recurrent excitatory circuits adapting to inactivity. *Nat. Neurosci.* **15**, 250–257 (2011).
14. Y. Wang *et al.*, Dlx5 and Dlx6 regulate the development of parvalbumin-expressing cortical interneurons. *J. Neurosci.* **30**, 5334–5345 (2010).
15. J. Dimidschstein *et al.*, A viral strategy for targeting and manipulating interneurons across vertebrate species. *Nat. Neurosci.* **19**, 1743–1749 (2016).
16. D. Zou *et al.*, DREADD in parvalbumin interneurons of the dentate gyrus modulates anxiety, social interaction and memory extinction. *Curr. Mol. Med.* **16**, 91–102 (2016).
17. B. R. Kanter *et al.*, A novel mechanism for the grid-to-place cell transformation revealed by transgenic depolarization of medial entorhinal cortex layer II. *Neuron* **93**, 1480–1492.e6 (2017).
18. R. Zhao *et al.*, Impaired recall of positional memory following chemogenetic disruption of place field stability. *Cell Rep.* **16**, 793–804 (2016).
19. C. Varela *et al.*, Tracking the time-dependent role of the hippocampus in memory recall using DREADDs. *PLoS One* **11**, e0154374 (2016).
20. A. Călin *et al.*, Chemogenetic recruitment of specific interneurons suppresses seizure activity. *Front. Cell. Neurosci.* **12**, 293 (2018).
21. Y. Wang *et al.*, Pharmaco-genetic therapeutics targeting parvalbumin neurons attenuate temporal lobe epilepsy. *Neurobiol. Dis.* **117**, 149–160 (2018).
22. B. O. Watson, M. Ding, G. Buzsáki, Temporal coupling of field potentials and action potentials in the neocortex. *Eur. J. Neurosci.* **48**, 2482–2497 (2018).
23. K. Mizuseki, G. Buzsáki, Preconfigured, skewed distribution of firing rates in the hippocampus and entorhinal cortex. *Cell Rep.* **4**, 1010–1021 (2013).
24. M. Stimberg, R. Brette, D. F. Goodman, Brian 2, an intuitive and efficient neural simulator. *eLife* **8**, e47314 (2019).
25. G. Buzsáki, C. A. Anastassiou, C. Koch, The origin of extracellular fields and currents—EEG, ECoG, LFP and spikes. *Nat. Rev. Neurosci.* **13**, 407–420 (2012).
26. J.-P. Lachaux, N. Axmacher, F. Mormann, E. Halgren, N. E. Crone, High-frequency neural activity and human cognition: Past, present and possible future of intracranial EEG research. *Prog. Neurobiol.* **98**, 279–301 (2012).
27. T. Klausberger, P. Somogyi, Neuronal diversity and temporal dynamics: The unity of hippocampal circuit operations. *Science* **321**, 53–57 (2008).
28. S. Royer *et al.*, Control of timing, rate and bursts of hippocampal place cells by dendritic and somatic inhibition. *Nat. Neurosci.* **15**, 769–775 (2012).
29. J. Csicsvari, H. Hirase, A. Czurkó, A. Mamiya, G. Buzsáki, Oscillatory coupling of hippocampal pyramidal cells and interneurons in the behaving rat. *J. Neurosci.* **19**, 274–287 (1999).
30. A. Ylinen *et al.*, Sharp wave-associated high-frequency oscillation (200 Hz) in the intact hippocampus: Network and intracellular mechanisms. *J. Neurosci.* **15**, 30–46 (1995).
31. G. Miesenböck, The optogenetic catechism. *Science* **326**, 395–399 (2009).
32. G. Buzsáki *et al.*, Tools for probing local circuits: High-density silicon probes combined with optogenetics. *Neuron* **86**, 92–105 (2015).
33. C. van Vreeswijk, H. Sompolinsky, Chaos in neuronal networks with balanced excitatory and inhibitory activity. *Science* **274**, 1724–1726 (1996).
34. D. J. Amit, N. Brunel, Model of global spontaneous activity and local structured activity during delay periods in the cerebral cortex. *Cereb. Cortex* **7**, 237–252 (1997).
35. R. Rubin, L. F. Abbott, H. Sompolinsky, Balanced excitation and inhibition are required for high-capacity, noise-robust neuronal selectivity. *Proc. Natl. Acad. Sci. U.S.A.* **114**, E9366–E9375 (2017).
36. A. Renart *et al.*, The asynchronous state in cortical circuits. *Science* **327**, 587–590 (2010).
37. D. G. Amaral, M. P. Witter, The three-dimensional organization of the hippocampal formation: A review of anatomical data. *Neuroscience* **31**, 571–591 (1989).
38. G. Fishell, B. Rudy, Mechanisms of inhibition within the telencephalon: "Where the wild things are." *Annu. Rev. Neurosci.* **34**, 535–567 (2011).
39. H. Markram, M. Tsodyks, Redistribution of synaptic efficacy between neocortical pyramidal neurons. *Nature* **382**, 807–810 (1996).
40. D. M. Kullmann, A. W. Moreau, Y. Bakiri, E. Nicholson, Plasticity of inhibition. *Neuron* **75**, 951–962 (2012).

41. N. J. Kopell, H. J. Gritton, M. A. Whittington, M. A. Kramer, Beyond the connectome: The dynome. *Neuron* **83**, 1319–1328 (2014).
42. G. Buzsáki, X.-J. Wang, Mechanisms of gamma oscillations. *Annu. Rev. Neurosci.* **35**, 203–225 (2012).
43. D. F. English *et al*., Pyramidal cell-interneuron circuit architecture and dynamics in hippocampal networks. *Neuron* **96**, 505–520.e7 (2017).
44. D. L. Buhl, G. Buzsáki, Developmental emergence of hippocampal fast-field "ripple" oscillations in the behaving rat pups. *Neuroscience* **134**, 1423–1430 (2005).
45. E. Stark *et al*., Pyramidal cell-interneuron interactions underlie hippocampal ripple oscillations. *Neuron* **83**, 467–480 (2014).
46. B. Chiovini *et al*., Dendritic spikes induce ripples in parvalbumin interneurons during hippocampal sharp waves. *Neuron* **82**, 908–924 (2014).
47. T. P. Vogels, H. Sprekeler, F. Zenke, C. Clopath, W. Gerstner, Inhibitory plasticity balances excitation and inhibition in sensory pathways and memory networks. *Science* **334**, 1569–1573 (2011).
48. Z. Nusser, N. Hájos, P. Somogyi, I. Mody, Increased number of synaptic GABA(A) receptors underlies potentiation at hippocampal inhibitory synapses. *Nature* **395**, 172–177 (1998).
49. W. C. Abraham, Metaplasticity: Tuning synapses and networks for plasticity. *Nat. Rev. Neurosci.* **9**, 387 (2008).
50. S. F. Owen *et al*., Oxytocin enhances hippocampal spike transmission by modulating fast-spiking interneurons. *Nature* **500**, 458–462 (2013).
51. A. Berényi *et al*., Large-scale, high-density (up to 512 channels) recording of local circuits in behaving animals. *J. Neurophysiol.* **111**, 1132–1149 (2014).
52. K. B. Hengen, A. Torrado Pacheco, J. N. McGregor, S. D. Van Hooser, G. G. Turrigiano, Neuronal firing rate homeostasis is inhibited by sleep and promoted by wake. *Cell* **165**, 180–191 (2016).
53. A. L. Reese, E. T. Kavalali, Spontaneous neurotransmission signals through store-driven Ca(2+) transients to maintain synaptic homeostasis. *eLife* **4**, e09262 (2015).
54. A. Bhatia, S. Moza, U. S. Bhalla, Precise excitation-inhibition balance controls gain and timing in the hippocampus. *eLife* **8**, e43415 (2019).
55. M. A. Gainey, D. E. Feldman, Multiple shared mechanisms for homeostatic plasticity in rodent somatosensory and visual cortex. *Philos. Trans. R. Soc. Lond. B Biol. Sci.* **372**, 20160157 (2017).
56. R. C. Froemke, Plasticity of cortical excitatory-inhibitory balance. *Annu. Rev. Neurosci.* **38**, 195–219 (2015).